PLOS BIOLOGY

RESEARCH ARTICLE

Effective polyploidy causes phenotypic delay and influences bacterial evolvability

Lei Sun[1‡], Helen K. Alexander[1¤‡], Balazs Bogos[1], Daniel J. Kiviet[2,3], Martin Ackermann[2,3], Sebastian Bonhoeffer[1]*

1 Institute of Integrative Biology, ETH Zürich, Zürich, Switzerland, **2** Institute of Biogeochemistry and Pollutant Dynamics, ETH Zürich, Zürich, Switzerland, **3** Department of Environmental Microbiology, Eawag, Swiss Federal Institute of Aquatic Science and Technology, Dübendorf, Switzerland

¤ Current address: Department of Zoology, University of Oxford, Oxford, United Kingdom
‡ These authors share first authorship on this work.
* seb@env.ethz.ch

Citation: Sun L, Alexander HK, Bogos B, Kiviet DJ, Ackermann M, Bonhoeffer S (2018) Effective polyploidy causes phenotypic delay and influences bacterial evolvability. PLoS Biol 16(2): e2004644. https://doi.org/10.1371/journal.pbio.2004644

Academic Editor: Arjan de Visser, Wageningen Universiteit en Researchcentrum, Netherlands

Received: October 27, 2017

Accepted: February 1, 2018

Published: February 22, 2018

Data Availability Statement: All relevant data are within the paper and its Supporting Information files. Additional material, consisting of computer codes and microscopic images, is available on the Dryad public repository: https://doi.org/10.5061/dryad.8723t.

Funding: European Research Council (grant number 268540). Received by SB. The funder had no role in study design, data collection and analysis, decision to publish, or preparation of the manuscript. Swiss National Science Foundation (grant number 155866). Received by SB. The

Abstract

Whether mutations in bacteria exhibit a noticeable delay before expressing their corresponding mutant phenotype was discussed intensively in the 1940s to 1950s, but the discussion eventually waned for lack of supportive evidence and perceived incompatibility with observed mutant distributions in fluctuation tests. Phenotypic delay in bacteria is widely assumed to be negligible, despite the lack of direct evidence. Here, we revisited the question using recombineering to introduce antibiotic resistance mutations into *E. coli* at defined time points and then tracking expression of the corresponding mutant phenotype over time. Contrary to previous assumptions, we found a substantial median phenotypic delay of three to four generations. We provided evidence that the primary source of this delay is multifork replication causing cells to be effectively polyploid, whereby wild-type gene copies transiently mask the phenotype of recessive mutant gene copies in the same cell. Using modeling and simulation methods, we explored the consequences of effective polyploidy for mutation rate estimation by fluctuation tests and sequencing-based methods. For recessive mutations, despite the substantial phenotypic delay, the per-copy or per-genome mutation rate is accurately estimated. However, the per-cell rate cannot be estimated by existing methods. Finally, with a mathematical model, we showed that effective polyploidy increases the frequency of costly recessive mutations in the standing genetic variation (SGV), and thus their potential contribution to evolutionary adaptation, while drastically reducing the chance that de novo recessive mutations can rescue populations facing a harsh environmental change such as antibiotic treatment. Overall, we have identified phenotypic delay and effective polyploidy as previously overlooked but essential components in bacterial evolvability, including antibiotic resistance evolution.

Author summary

What is the time delay between the occurrence of a genetic mutation in a bacterial cell and manifestation of its phenotypic effect? We show that antibiotic resistance mutations

funder had no role in study design, data collection and analysis, decision to publish, or preparation of the manuscript. Swiss National Science Foundation (grant number 31003A_149267). Received by MA. The funder had no role in study design, data collection and analysis, decision to publish, or preparation of the manuscript. ETH Zurich. The funder had no role in study design, data collection and analysis, decision to publish, or preparation of the manuscript.

Competing interests: The authors have declared that no competing interests exist.

Abbreviations: CFU, colony-forming unit; lac$^-$, lactose auxotrophy; lac$^+$, lactose prototrophy; MA, mutation accumulation; MIC, minimum inhibitory concentration; MLE, maximum likelihood estimate; NalR, nalidixic acid resistance; RifR, rifampicin resistance; SGV, standing genetic variation; ssDNA, single-stranded DNA; StrepR, streptomycin resistance; WGS, whole-genome sequencing; YFP, yellow fluorescent protein.

in *Escherichia coli* show a remarkably long phenotypic delay of three to four bacterial generations. The primary underlying mechanism of this delay is effective polyploidy. If a mutation arises on one of the multiple chromosomes in a polyploid cell, the presence of nonmutated, wild-type gene copies on other chromosomes may mask the phenotype of the mutation. We show here that mutation rate estimation needs to consider polyploidy, which influences the potential for bacterial adaptation. The fact that a new mutation may become useful only in the "great-great-grandchildren" suggests that preexisting mutations are more important for surviving sudden environmental catastrophes.

Introduction

As genetic mutations appear on the DNA, their effects must first transcend the RNA and protein levels before resulting in an altered phenotype. This so-called "phenotypic delay" in the expression of new mutations could have major implications for evolutionary adaptation, particularly if selection pressures change on a timescale that is short relative to this delay, as may be the case for selection by antibiotics. The duration of phenotypic delay is an old but nearly forgotten question in microbiology[1–3]. Luria and Delbrück were interested in the delay because they expected it to affect the mutant distribution in the fluctuation test in their seminal work on the random nature of mutations [1]. They argued that if a mutant clone expressed its phenotype after G generations, then phenotypic mutants should be observed in populations in groups of 2^G. Frequent observations of single-mutant populations, however, suggested $G \approx 0$. They therefore concluded that the phenotypic delay is negligible [1,3,4]. This has remained the modus operandi [4], despite the fact that molecular cloning protocols imply a significant delay because they require a waiting time typically longer than a bacterial generation to express new genetic constructs [5].

To quantify the phenotypic delay more directly, the time point of occurrence of a mutation in a cell needs to be known, which has only become possible with modern methods of genetic engineering. Here, we use a recombineering approach to introduce mutations in *E. coli* within a narrow time window and find a remarkable phenotypic delay of three to four generations for three antibiotic resistance mutations. We identify the underlying mechanism as effective polyploidy, which reconciles the long phenotypic delay with Luria and Delbrück's observations. Investigating the consequences of effective polyploidy and phenotypic delay, we find that mutation rate estimates need to be adjusted for ploidy. Moreover, resistance mutations that occur after exposure to antibiotics are much less likely to survive due to the multigenerational phenotypic delay, while preexisting mutations become a much more important contributor to survival.

Results

Mutations in bacteria exhibit multigenerational phenotypic delay

To quantify phenotypic delay, we introduced each of four mutations at a specified time point in *E. coli* with an optimized recombineering protocol (Materials and methods), in which a single-stranded DNA (ssDNA) oligonucleotide carrying the point-specific mutation is transformed into bacteria by electroporation [6]. The ssDNA then binds reverse complementarily to its target on the bacterial genome as part of a lagging strand in an open replication fork [6], thereby introducing the mutation. Three mutations confer antibiotic resistance to rifampicin, nalidixic acid and streptomycin, respectively (RifR, NalR, and StrepR) [7]; the fourth mutation

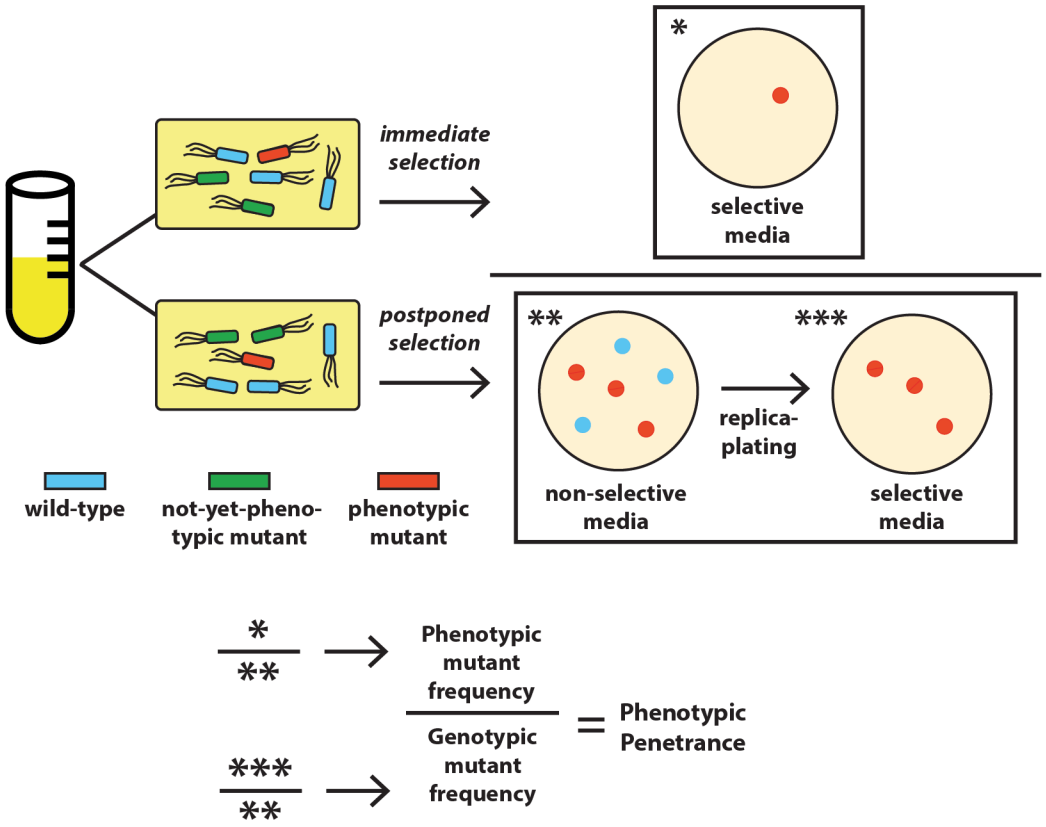

Fig 1. Schematic illustration of the quantification of phenotypic penetrance.

https://doi.org/10.1371/journal.pbio.2004644.g001

enables lactose prototrophy (lac$^+$) [8] (S1 Table). After introduction of the mutations, the cells grew continuously without selection and were sampled over time. Sampled cells were subjected to "immediate" versus "postponed" selection to quantify, respectively, the frequencies of current phenotypic mutants and of genotypic mutants (that contain at least one mutant gene copy and eventually have some phenotypic mutant descendants), with their ratio called phenotypic penetrance (Fig 1). Phenotypic delay is quantified as the time in bacterial generations to reach 50% phenotypic penetrance.

Surprisingly, all three resistance mutations showed significant phenotypic delay at two selective concentrations of their respective antibiotic (Fig 2A). Reaching 50% phenotypic penetrance required five to six generations of postrecombineering growth. The frequency of genotypic mutants increased over the first one to two generations but eventually declined (Fig 2C). The transient increase may reflect the time window of introduction of the mutations. Discounting the first two generations, a phenotypic delay of three to four generations remains to be explained.

Effective polyploidy is the primary source of phenotypic delay

Phenotypic delay could result from multiple factors. Firstly, it could arise from the gradual replacement of wild-type proteins by mutant proteins following mutagenesis. Time may be required for sufficient protein turnover before the mutant phenotype can manifest. Another possibility is that cells are effectively polyploid due to multifork replication [9,10]. Recombineering incorporates the mutation into only one or some of the chromosomes starting from a

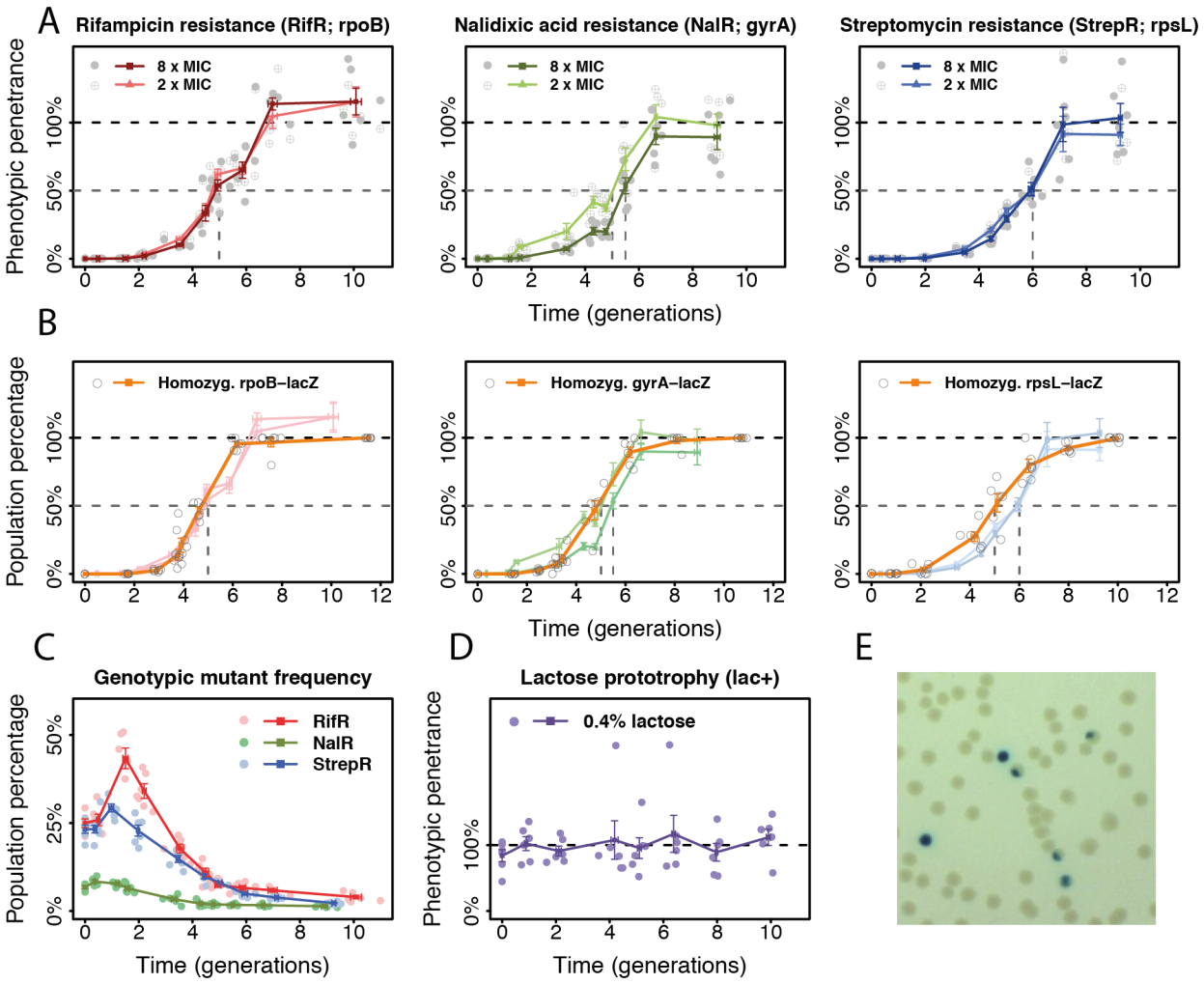

Fig 2. Phenotypic delay in *E. coli*. (A) Phenotypic penetrance (mean ± SE; $n = 6$) over time for three antibiotic resistance mutations. Gray dashed lines: time at 50% phenotypic penetrance. (B) Frequency of homozygous mutants among all mutants (orange) for the three resistance mutations assessed by *lacZ* reporter constructs (*rpoB-lacZ*, *gyrA-lacZ*, *rpsL-lacZ*), overlaid with their respective phenotypic penetrance. (C) Genotypic mutant frequency for the resistance mutations. (D) Phenotypic penetrance of the lactose prototrophy (*rpsL-lacZ*) mutation. (E) Colonies founded by homozygous (blue) and heterozygous (sectored) lac$^+$ mutants. The numerical data for panels A to D can be found in S1 Data. MIC, minimum inhibitory concentration.

https://doi.org/10.1371/journal.pbio.2004644.g002

single-strand mutant DNA [6], comparable to the occurrence of natural mutations. This yields effectively heterozygous cells that could produce both wild-type and mutant proteins from different chromosomes, which may prevent the onset of the mutant phenotype. Three generations could be the minimal time needed for a cell with one mutant copy out of eight chromosomes (comparable to previous estimates [9]) to produce the first homozygous mutant carrying only mutant alleles. Effective polyploidy is also compatible with the observed decline in genotypic mutant frequency (Fig 2C) because heterozygous mutants produce both mutant and wild-type descendants, such that the frequency of cells carrying at least one mutant gene copy will decline until all cells are homozygous.

To quantify the contribution of effective polyploidy, we used a *lacZ* reporter assay to visualize heterozygous mutants. We constructed three reporter strains with a disrupted *lacZ* gene inserted close to each resistance target gene and restored it through recombineering

(S2 Table). Genotypic mutants were visualized by plating on indicator media where lac^+ and lac^- cells become blue and white, respectively. Heterozygous mutants generate sectored colonies, while homozygous mutants generate blue colonies, thus indicating the frequency of homozygous mutants amongst all genotypic mutants (Fig 2E). Comparing the estimated proportion of homozygous reporter mutants with the corresponding phenotypic penetrance of the resistance mutation reveals that phenotypic delay can be fully explained by effective polyploidy for NalR at 2x minimum inhibitory concentration (MIC) and for RifR (Fig 2B). Homozygosity precedes phenotypic penetrance by about 0.5 generations for NalR at 8x MIC and one generation for StrepR, suggesting that here, additional protein turnover may be involved.

These results also imply that these resistance mutations are genetically recessive to antibiotic sensitivity, which has also been described in previous studies based on co-expression assays [11,12]. The recessive nature of these antibiotic resistance alleles stems from their molecular mechanism: when the antibiotic molecule binds to its target protein, the resulting complex is capable of damaging the cell even in small quantities, essentially acting as toxins. As a result, the gene dosage of wild-type targets is critical. For instance, nalidixic acid-bound gyrase proteins can introduce DNA double-stranded breaks [13]. In particular, bacteria that overexpress gyrase become even more sensitive to quinolone antibiotics [14]. Although the exact killing mechanism of streptomycin remains a subject of debate, it is generally accepted that streptomycin-bound ribosomes damage the cell via mistranslation [15]. Finally, rifampicin-bound RNA polymerase appears to blockade the DNA, thereby preventing transcription even by drug-resistant RNA polymerases [12]. Although dominant RifR mutations have also been described [16], the mutation we tested here appears to be recessive.

In the case of *lacZ* mutations, we scored the frequency of lac^+ phenotypic mutants on lactose-limited media. The ability to metabolize lactose is dominant to its inability [8]. Because any cell containing a lac^+ allele can metabolize lactose and eventually form a colony, phenotypic penetrance, as expected, was always at 100% (Fig 2D), indicating that the observed phenotypic delay of resistance mutations is not an artifact of our protocol.

Effective polyploidy causes asymmetrical inheritance of mutations

A further testable prediction of effective polyploidy is that inheritance of mutant alleles is asymmetrical: heterozygous mutants are expected to produce both wild-type and mutant offspring. For mutations with intermediate dominance, offspring progressing towards mutant homozygosity should show an increasingly mutant phenotype, while others show a transient phenotype because they inherit no mutant genes and their mutant proteins are diluted over subsequent divisions. Phenotypic delay would manifest as the time such mutations need to reach full phenotypic expression. To test this prediction, we repaired a disrupted *YFP* gene with recombineering, creating fluorescent mutants where the fluorescence intensity depends on the number of functional copies of this gene. We then tracked fluorescence as an intermediate-dominant phenotypic trait using single-cell imaging. As expected, we observed fully, transiently, and non-fluorescent offspring lineages from recombineering-treated cells (Fig 3A–3C, S1 Movie), consistent with effective polyploidy. Furthermore, fluorescence in mutant lineages increased monotonically and reached maximal intensity almost two generations after forming homozygous mutants (Fig 3C). This additional delay could be due to protein folding [17]. In total, we found 34 homozygous mutant lineages in 25 microcolonies. Six microcolonies spawned multiple, separate homozygous mutant lineages, thus corroborating previous findings that recombineering may modify multiple genome copies in one cell [18]. Overall, a median of five generations was required to form homozygous mutants, consistent with our

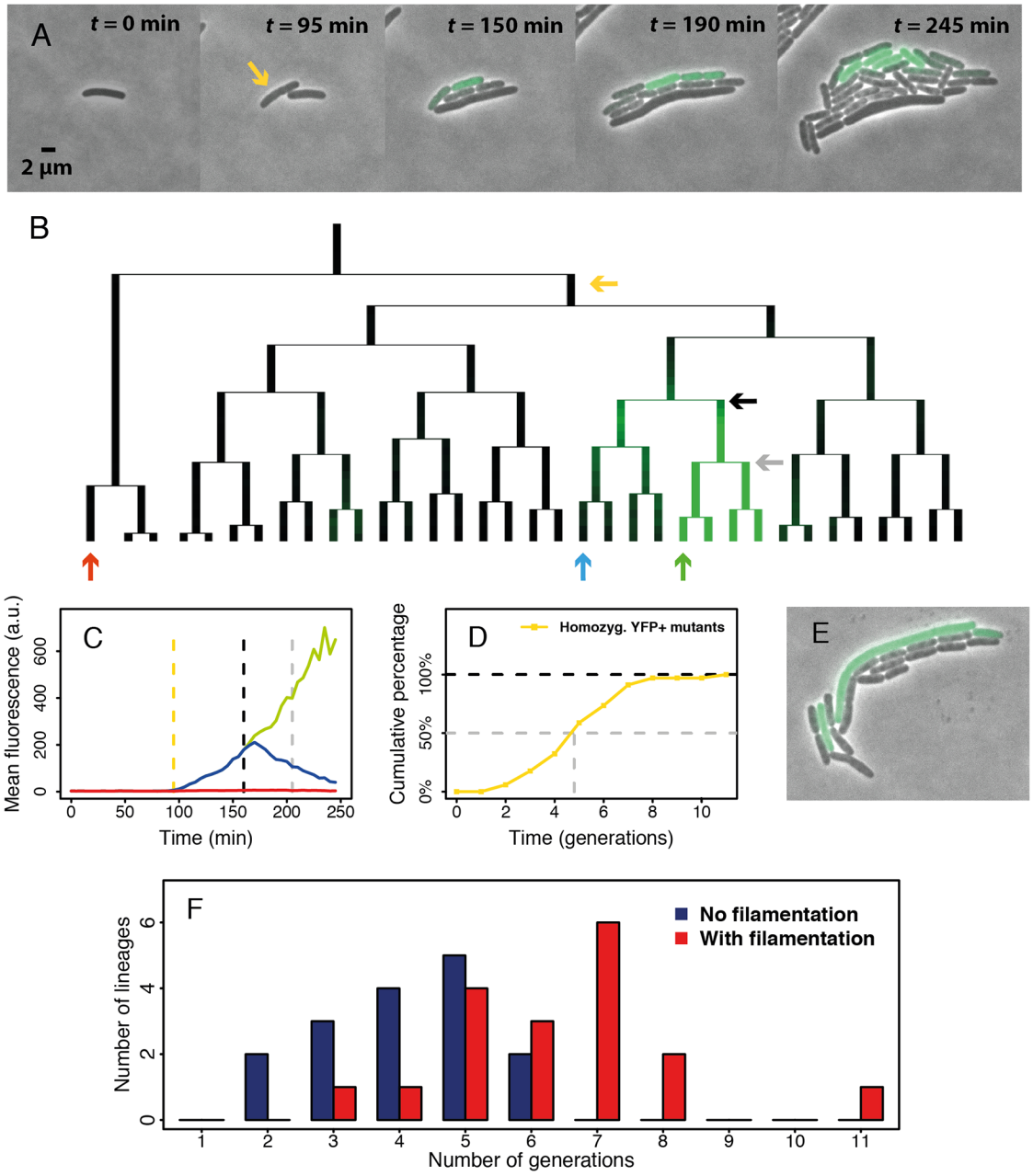

Fig 3. Single-cell analysis of fluorescent mutants. (A) Overlay of phase-contrast and fluorescence images showing a microcolony containing fluorescent mutants (see also S1 Movie). Yellow arrow: the first cell showing significantly higher fluorescence than background in the given frame. Accounting for the time required for YFP protein folding and maturation, the ssDNA integration is estimated to have happened before the first division of the labeled cell. (B) Genealogy of the aforementioned microcolony. The yellow arrow indicates the cell in A, while the remaining arrows indicate three lineages in which fluorescence was quantified. (C) YFP expression history of three lineages in B showing fully, transiently, and non-fluorescent phenotypes (green, blue, and red, respectively). Yellow dashed line: onset of fluorescence. Black and grey dashed lines correspond to the black and grey arrows in B. Black: emergence of the first homozygous mutant; grey: its first division. (D) Distribution of time to form 34 homozygous mutant lineages from 25 microcolonies. The data are obtained by directly analyzing genealogies as in B and compiled from two separate experiments. The dashed grey line indicates the estimated generations to form half of the homozygous mutant lineages. (E) Photo of a microcolony with one filamentous fluorescent cell. (F) The distribution of number of generations to form homozygous mutant lineages sorted by the presence/absence of filamentation. The numerical data for panels C, D, and F can be found in S1 Data. ssDNA, single-stranded DNA; YFP, yellow fluorescent protein.

https://doi.org/10.1371/journal.pbio.2004644.g003

lacZ reporter assay results (Fig 3D). These results provide direct visual support that effective polyploidy underlies phenotypic delay. A similar pattern has been observed previously in *E. coli* with fimbrial switching, a genetic modification that involves inversion of a promoter sequence on the bacterial genome [19].

Electroporation, as used in the recombineering protocol, may cause bacteria to form filaments due to stress [20]. Filamentation might exacerbate phenotypic delay by increasing the intracellular genome copy number. Our single-cell experiment revealed that filamentation was indeed frequent (Fig 3E). By directly observing the cell shape and the time point for onset of fluorescence, we estimated that 18 out of 34 homozygous mutant lineages incorporated the ssDNA mutation into a filamentous ancestor cell. Strikingly, lineages initiated by filamentous cells showed a distinctly different distribution of time to form the first homozygous mutant than nonfilamentous lineages (Fig 3F). Nonfilamentous lineages showed a median of 4 generations until homozygosity, as would be required for cells that incorporated the mutation in 1 out of 16 DNA single strands (i.e., 8 chromosomes) in less than 1 generation post recombineering. In contrast, filamentous lineages showed a median of 6.5 generations, and all lineages requiring more than 6 generations were filamentous. In conclusion, both filamentous and nonfilamentous cells exhibit a multigenerational phenotypic delay. Filamentation, however, can exacerbate phenotypic delay presumably by increasing the number of chromosome copies within a cell, explaining particularly long delays of extensive generations sometimes observed in our experiments.

Effects of chromosomal location on mutagenesis and delay

Because phenotypic delay arises from effective polyploidy, one would expect genes further from the replication origin with lower ploidy than origin-proximal genes to show shorter phenotypic delay. However, we observed a similar phenotypic delay and distribution of time until homozygosity for all three tested genes (Fig 2) despite different distances from the origin. Further analysis revealed a strong negative correlation between distance to origin and the initial frequency of genotypic mutants induced by recombineering (Fig 4A and 4B). We hypothesized that these observations reflect the mechanism of mutagenesis by recombineering. Because open replication forks are required for recombineering, mutations could only be introduced during DNA replication [21]. The probability of successful mutagenesis on at least one open chromosomal target increases with ploidy, which itself increases during DNA replication. Therefore, we hypothesized that instead of mutating at low ploidy and thereby exhibiting shorter phenotypic delay, most of our observed origin-distal mutations were generated when their targets transiently reached higher ploidy either during normal DNA replication or due to cell filamentation. Therefore, consistent with our observations so far, origin-distal mutations would show phenotypic delay similar to origin-proximal mutations but reduced recombineering efficiency because origin-distal genes are less accessible for mutagenesis.

To further test this hypothesis, we inferred a minimal ploidy of the aforementioned target sites at the precise time point of ssDNA integration with an adapted *lacZ* reporter assay that measured the fraction of mutant cells in mutant colonies directly after recombineering (Materials and methods). Overall, the distributions of ploidy were similar for the three tested chromosomal locations at 5.5%, 9.7%, and 34.2% genome distance from the origin (Fig 4C). This result potentially explains why we observed no effect of chromosomal location on phenotypic delay. Furthermore, this principle should apply not only to recombineering but also to natural mutations that arise during DNA replication.

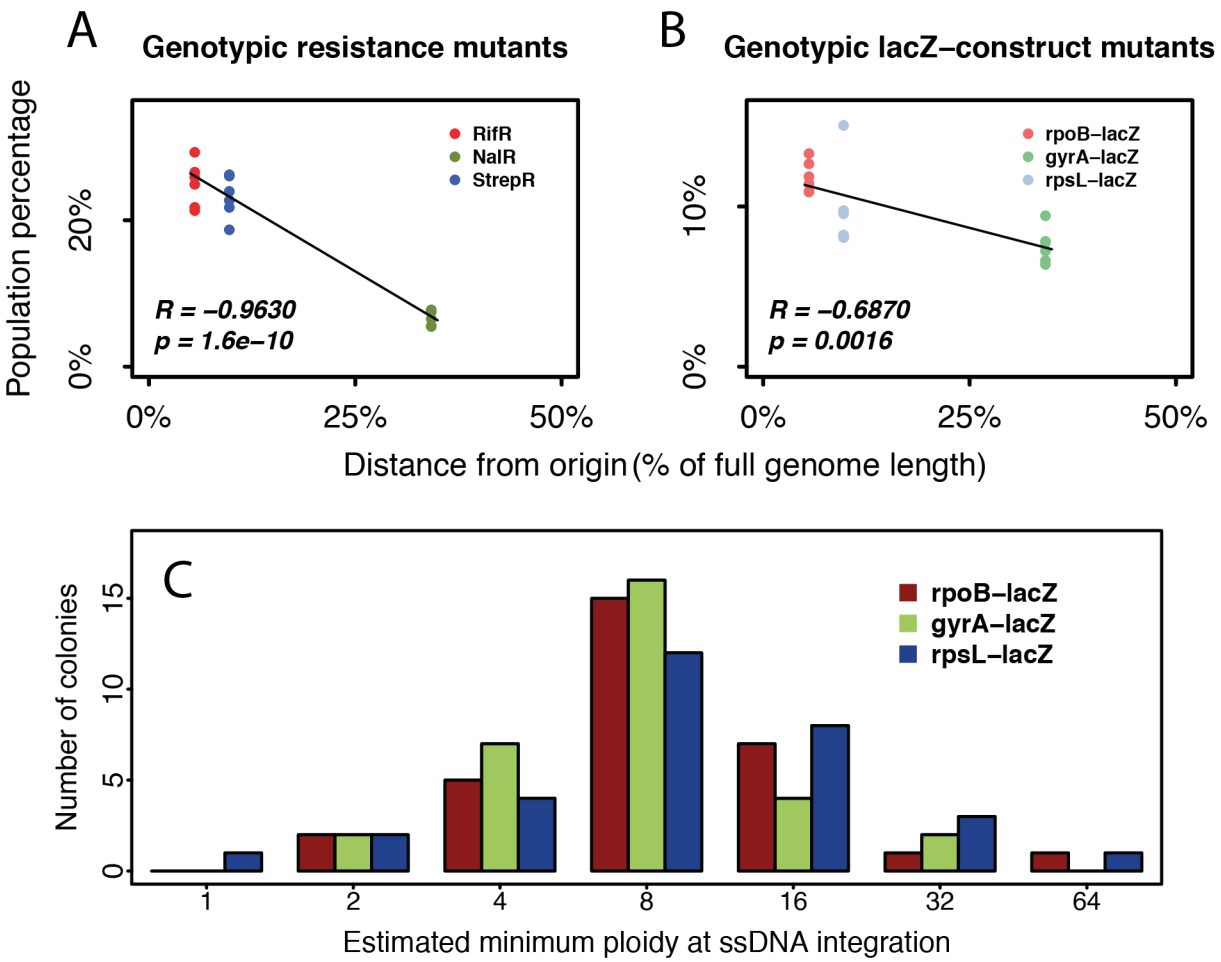

Fig 4. Chromosomal location effects on recombineering. Resistance target genes rpoB, gyrA, and rpsL are at 5.5%, 34.2%, and 9.7% genomic distance from the replication origin, respectively. Strong negative correlation (quantified by Pearson's correlation coefficient, R) exists between the distance from the origin and the initial frequency of genotypic mutants induced by recombineering, for both (A) the resistance mutations and (B) their *lacZ* reporters. (C) The inferred minimal ploidy from the cell physically treated by recombineering at the time of mutant ssDNA integration shows a similar distribution for all constructs, regardless of their distance from the origin ($n = 31$ colonies examined per construct). Eight is the median and the most common inferred minimum ploidy, consistent with previous estimates of ploidy in *E. coli* [10,22]. Higher estimates of 16, 32, and 64 could have resulted from delayed ssDNA integration or ssDNA integration in a filamentous cell. The numerical data can be found in S1 Data. ssDNA, single-stranded DNA.

https://doi.org/10.1371/journal.pbio.2004644.g004

Effective polyploidy and phenotypic delay affect mutation rate estimation

Fluctuation tests are widely used to estimate bacterial mutation rates by counting mutants exhibiting a selectable phenotype. Selection is typically applied to stationary phase cells [23], which are expected to be polyploid [10,22]. That polyploidy should affect the appearance of mutants in the fluctuation test was already pointed out quite early in the literature [24,25], but subsequently this consideration largely fell by the wayside.

When a mutation arises in an effectively polyploid cell, the first homozygous mutant descendant must appear as a single cell in the population (Fig 5). Therefore, in contrast with earlier interpretations [1], the frequent observation of singletons in the mutant distribution does not invalidate the existence of a substantial phenotypic delay. Furthermore, because heterozygous cells carrying recessive mutations do not exhibit the mutant phenotype, i.e., cannot form colonies on selective plates in the fluctuation test, these unobserved mutants should result

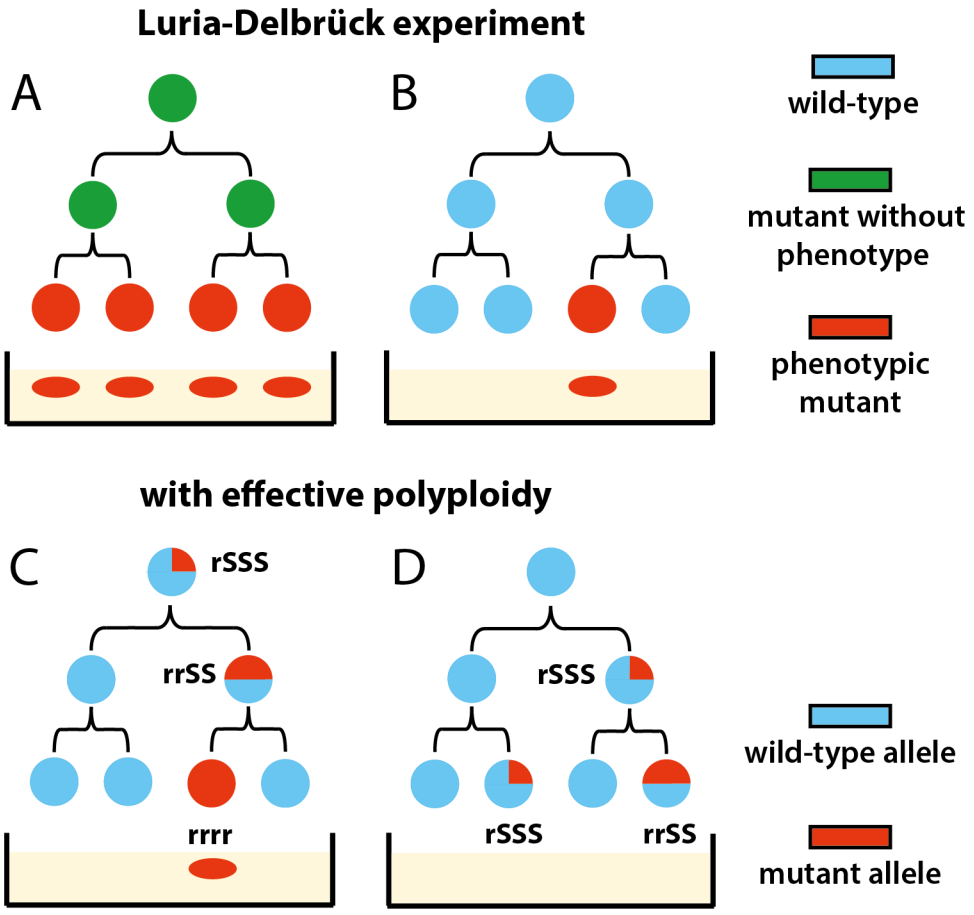

Fig 5. Reconciling Luria-Delbrück fluctuation test with phenotypic delay by effective polyploidy. (A) The original Luria-Delbrück mutation model disregards polyploidy. For instance, a phenotypic delay of two generations results in four mutants appearing at once. (B) The observation of many one-mutant ("singleton") populations was interpreted as evidence against the existence of a delay [1,3]. (C) With polyploidy considered, cells with four genome copies require two divisions to generate a homozygous mutant that expresses a selectable recessive phenotype. Therefore, a delay of two generations can generate just one mutant. (D) Heterozygous cells containing recessive mutations will not survive selection, leading to an underestimation of mutational events.

https://doi.org/10.1371/journal.pbio.2004644.g005

in an underestimation of the mutation rate. Incidentally, the phage or antibiotic resistance mutations typically used in fluctuation tests are recessive [11,12,26].

The impact of polyploidy on mutation rate estimation from fluctuation tests using the modern "gold standard" maximum likelihood method [23] has not been examined. Although one recent study considered the "segregation lag" for recessive mutations resulting from polyploidy [27], corrections to mutation rate estimators were only derived for two simpler methods with limited range of accuracy and low statistical efficiency relative to the maximum likelihood method [23]. Furthermore, these derivations neglected the key point that not all descendants of heterozygous mutants will be mutants themselves.

We investigated the effect of polyploidy on observed mutant distributions, and thus estimated mutation rates, for both dominant and recessive mutations by simulating fluctuation tests. Our simulation model assumed fixed effective ploidy at the target by doubling and symmetrically dividing chromosome copies upon division according to a model of segregation that is justified for *E. coli* (Materials and methods). Importantly, this model leads to the shortest possible time to homozygosity and thus a conservative estimate of lag; however, other

models of segregation in bacteria and archaea are possible [27,28]. From simulated cultures, we counted phenotypic mutants given either a completely dominant or a completely recessive mutation, assuming instant protein equilibration, and estimated mutation rates using standard maximum likelihood methods [23,29,30]. Other than polyploidy and dominance considerations, all modelling assumptions are the same as the standard approach (Materials and methods), allowing us to isolate the effect of ploidy. Under our model, ploidy c has two effects relative to monoploidy: (i) it increases the number of mutation targets and thus the per-cell mutation rate by a factor c, and (ii) it generates initially heterozygous mutants that, after a delay of $\log_2 c$ generations, produce one out of c homozygous mutant descendants (S1 Fig).

The mutation rate estimate at the mutational target can be compared to the actual per-copy rate μ_c and per-cell rate $c \cdot \mu_c$ used in the simulations (Fig 6A and 6B). When $c = 1$ (monoploidy), as the standard method assumes, the estimate indeed reflects the per-copy or (equivalently) per-cell rate. For $c > 1$, the estimate is higher for dominant than for recessive traits. Surprisingly, for recessive traits, the estimate tends to coincide with the per-copy rate μ_c regardless of ploidy. For dominant traits, the estimate lies between the per-copy and per-cell rates, with confidence interval size increasing with ploidy. These patterns are robust across a range of parameter values (S2 Fig). In fact, these effects have a precise mathematical explanation (S1 Text section 2.2): the distribution of mutant counts in a polyploid population turns out to match the standard (monoploid) model with rescaled mutational influx in the case of a recessive trait (Fig 6C and S3A Fig) but fundamentally differs for a dominant trait (Fig 6D and S3B Fig). Therefore, for more commonly used recessive traits, estimates reflect mutation rates per target copy, which can be scaled up to per genome copy. This could explain why per-nucleotide mutation rates estimated from different targets do not differ significantly, despite differences in target location that potentially influence their copy number [31].

We then asked whether effective polyploidy impacts mutation rate estimates based on whole-genome sequencing (WGS) as well as fluctuation tests. WGS is typically conducted on evolved populations from mutation accumulation (MA) assays, which use single-cell bottlenecking to minimize selection [31]. Under the simplifying assumptions of fixed generation time and no cell death, we modeled an MA assay by tracking the single lineage that passes through each bottleneck and is ultimately sampled for sequencing (S1 Text section 3 and S4 Fig). Accounting for polyploidy, the per-cell mutation rate is $c \cdot \mu_g$, where μ_g is the per-genome-copy mutation rate. However, due to asymmetric inheritance, only a fraction $1/c$ of descendants from a mutant progenitor will eventually become homozygous mutants. Therefore, only a fraction $1/c$ of mutations arising in the focal lineage will ultimately be sampled, leaving the per–genome copy rate μ_g as the inferred mutation rate (S1 Text section 3). We therefore conclude that neither the fluctuation test nor WGS methods can accurately capture the per-cell mutation rate. Therefore, as the typical assumption is one genome per cell, neglecting polyploidy underestimates the total influx of de novo mutations in bacterial populations, which is relevant for adaptation.

Polyploidy and phenotypic delay impact bacterial evolvability under selection

Effective polyploidy has important consequences for evolutionary adaptation, both through the aforementioned increased influx of mutations and the masking of recessive mutations' phenotype. Masking of deleterious recessive mutations is expected to increase their frequency in the standing genetic variation (SGV) and yield transiently lower, but eventually higher, mutational load in a fixed environment [28,32]. This higher standing frequency could promote adaptation to new environments should these mutations become beneficial. However, in an

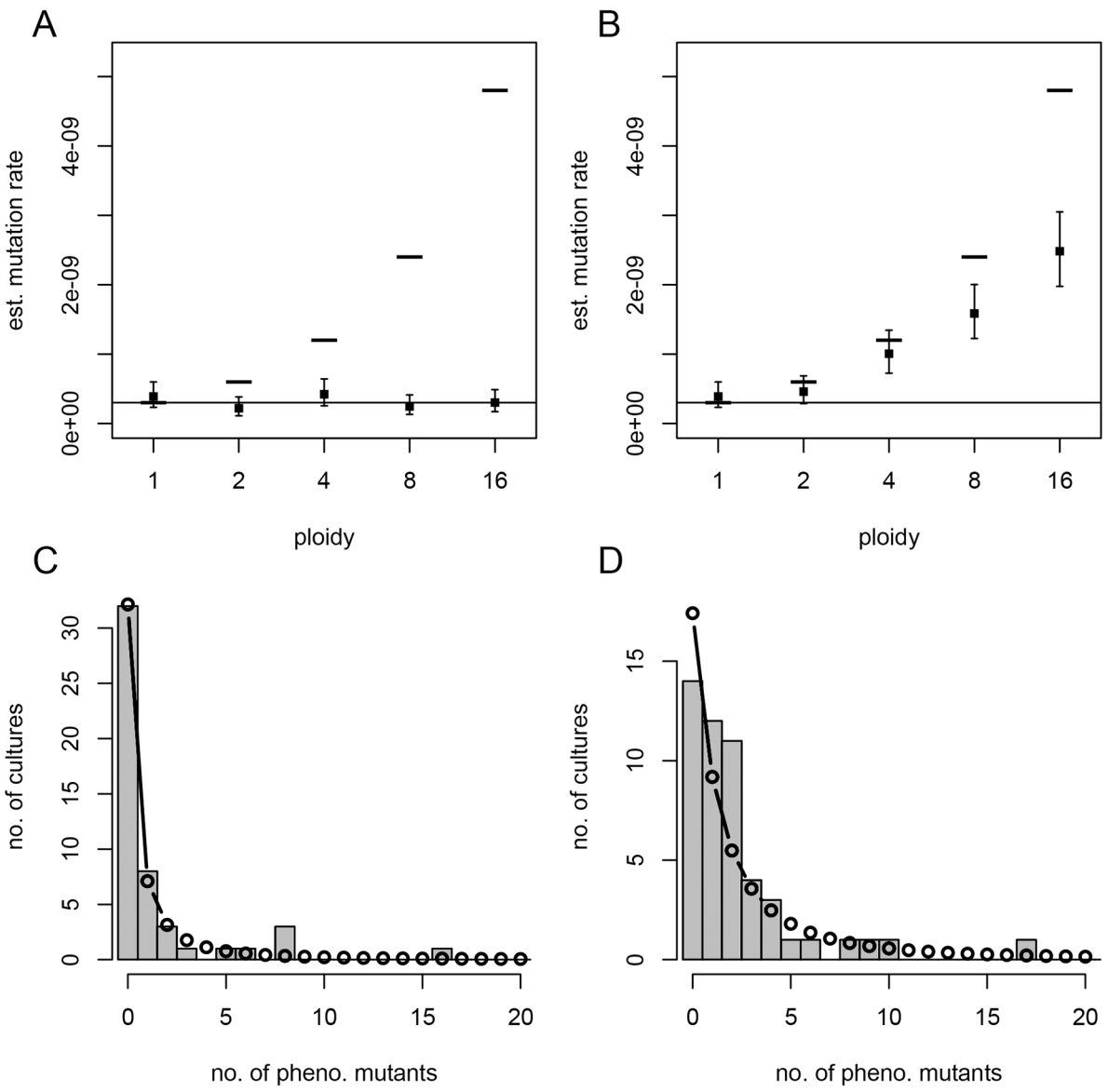

Fig 6. Simulated fluctuation tests. Mutation rate estimates (MLEs, filled squares; and 95% confidence intervals, error bars) from 50 simulated parallel cultures at each ploidy (c), with constant mutant interdivision time, assuming either a recessive (A) or dominant (B) mutation. The lower solid line and upper dashes indicate the per-copy ($\mu_c = 3 \times 10^{-10}$) and per-cell ($c \cdot \mu_c$) mutation rates, respectively, used for simulation. For $c = 4$ and recessive (C) or dominant (D) mutations, the observed mutant count distribution (histogram) is compared to that predicted by the standard model parameterized by the MLE mutation rate (connected points). This figure can be reproduced using code and simulated data deposited on Dryad (http://dx.doi.org/10.5061/dryad.8723-t). MLE, maximum likelihood estimate.

https://doi.org/10.1371/journal.pbio.2004644.g006

environment where mutations are beneficial, masking their effects should hinder adaptation. Previous theoretical studies addressing these conflicting effects of ploidy on adaptation [32,33] have not been linked to bacteria, nor have they specifically considered the chance of evolutionary rescue, i.e., rapid adaptation preventing extinction under sudden harsh environmental change (e.g., antibiotic treatment).

Rescue mutations may preexist in the SGV and/or arise de novo after the environmental shift during residual divisions of wild-type cells. The source of rescue mutations has implications for the optimal approach to drug treatment [34] and the preservation of genetic diversity

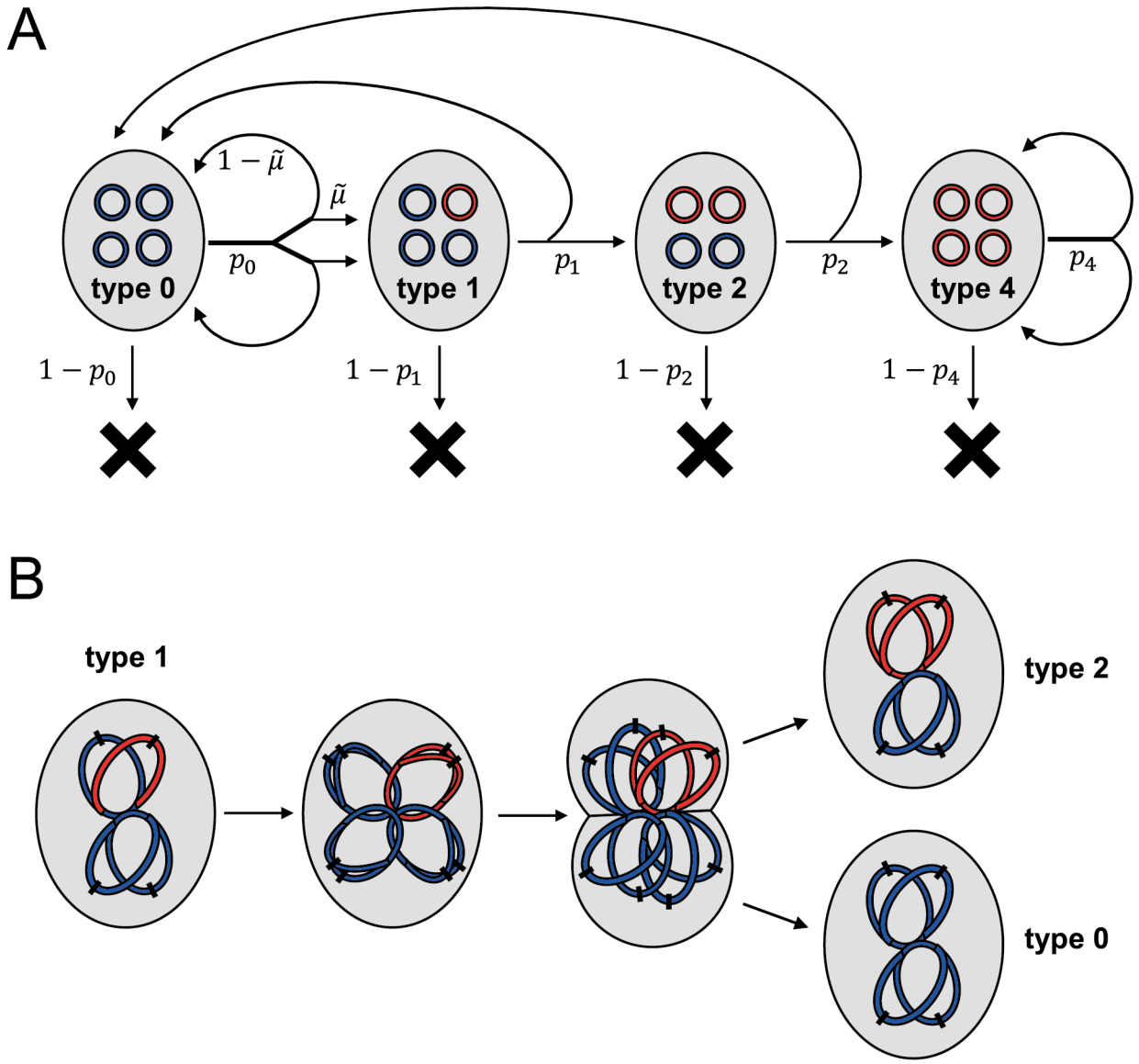

Fig 7. Schematic of the model used to evaluate SGV and rescue, illustrated for ploidy $c = 4$. (A) Flow diagram of all events. A cell is represented by a grey oval, containing four chromosomes (complete or partial, so long as they contain the gene of interest). These chromosomes are colored blue if wild-type at the gene of interest or red if mutant. A cell either divides to produce two daughter cells with type-specific probability p_j or otherwise dies. These probabilities p_j differ between the old environment (to model SGV) and the new environment (to model rescue). Upon type 0 division, mutation (producing type 1) occurs with probability $\tilde{\mu}$ in each daughter cell; otherwise, the daughter is also type 0. In the remaining types, chromosome segregation determines the types of the daughter cells. (B) A mechanistic view of chromosome replication and segregation, illustrated for the production of one type 2 and one type 0 daughter cell from a type 1 mother cell. On each chromosome, the black dash indicates the origin of replication. SGV, standing genetic variation.

https://doi.org/10.1371/journal.pbio.2004644.g007

following rescue [35]. To address the impact of effective polyploidy on rescue from SGV and de novo mutations, we developed a mathematical model of replication, mutations, and chromosome segregation in polyploid bacterial cells (Fig 7 and S1 Text section 4).

We first derived the frequency of mutants in the SGV at mutation–selection balance in the "old" environment, where mutations continually arise at rate $\tilde{\mu}_c$ per chromosome copy per replication and, if expressed, carry a fitness cost s (S1 Text section 4.2). This yielded analytical

Table 1. Approximate mutant frequencies at mutation–selection balance. Ploidy is $c = 2^n$ ($n \geq 1$) in the polyploid cases, $\tilde{\mu}_c$ is the per-copy mutation rate, and s is the cost of the mutation in homozygotes (in heterozygotes, the cost is masked in the recessive case but expressed in the dominant case).

	Monoploid	Polyploid recessive	Polyploid dominant
Frequency of heterozygous mutant cells (2^i mutant chroms., $0 \leq i \leq n-1$)	–	$2^{n-i}\tilde{\mu}_c$	$(1-s)^i \ 2^{n-i} \ \tilde{\mu}_c$
Frequency of homozygous mutant cells ($2^n = c$ mutant chroms.)	$\tilde{\mu}_c/s$	$\tilde{\mu}_c/s$	$(1-s)^n \ \tilde{\mu}_c/s$
Total frequency of mutant allele	$\tilde{\mu}_c/s$	$(n-1)\tilde{\mu}_c + \tilde{\mu}_c/s$	$\tilde{\mu}_c/s$

https://doi.org/10.1371/journal.pbio.2004644.t001

expressions confirming that polyploidy increases the total frequency of a recessive mutant allele by masking its cost in heterozygotes. In contrast, the total mutant allele frequency is independent of ploidy if the mutation is dominant (Table 1 and S5 Fig).

Next, we considered the fate of the population upon shifting to a new, harsh environment (e.g., antibiotic treatment), where phenotypically wild-type ("sensitive") cells have a low probability of successfully dividing while phenotypically mutant ("resistant") cells have a higher probability. The population may already contain heterozygous and homozygous mutants in the SGV and additionally give rise to de novo mutants stochastically according to a Poisson process. We developed a branching process model to evaluate the probability that such mutations escape stochastic extinction, accounting in particular for the multiple cell divisions required until mutations segregate to homozygosity, with probabilities of successful division depending on whether these mutations are recessive or dominant. Finally, combining these model components yielded expressions for the probability of population rescue from SGV, P_{SGV}, and from de novo mutations, P_{DN} (S1 Text section 4.3).

These rescue probabilities depend strongly on ploidy, dominance, and other model parameters (Fig 8, S6, S7, S8 and S9 Figs). In the recessive case, if phenotypically wild-type cells cannot divide in the new environment (e.g., a perfectly effective antibiotic), then P_{SGV} is independent of ploidy, reflecting the constant frequency of preexisting phenotypically mutant homozygotes (Table 1). This result is consistent with our above findings for fluctuation tests. If division of wild-type cells is possible (e.g., imperfect antibiotic efficacy), then P_{SGV} increases with ploidy because heterozygotes may produce additional homozygous mutant descendants. On the other hand, P_{DN} decreases with ploidy because de novo mutations require more cell divisions until segregation is complete and the mutant phenotype is expressed, which turns out to outweigh the increase in mutational influx (S1 Text). Therefore, although the overall probability of rescue remains similar as ploidy increases, rescue is increasingly from SGV rather than de novo mutations (Fig 8A and 8B). These qualitative patterns are robust to variations in the model parameters (S6 and S8 Figs). For dominant mutations, on the other hand, both P_{SGV} and P_{DN} increase with ploidy, and their relative contributions can show more complex patterns (Fig 8C and 8D, S7 and S9 Figs). In general, SGV makes a relatively larger contribution when the mutation has a low cost in antibiotic-free conditions (small s) and when the antibiotic is highly effective (low p_S), in agreement with previous findings in the evolutionary rescue literature [36].

Discussion

The phenotypic effect of a bacterial mutation cannot manifest instantaneously. Here, we therefore asked two questions: how large is this phenotypic delay, and what is its primary cause? We found a delay of three to four generations in the expression of three recessive antibiotic resistance mutations in *E. coli* and provided evidence that effective polyploidy is its primary cause.

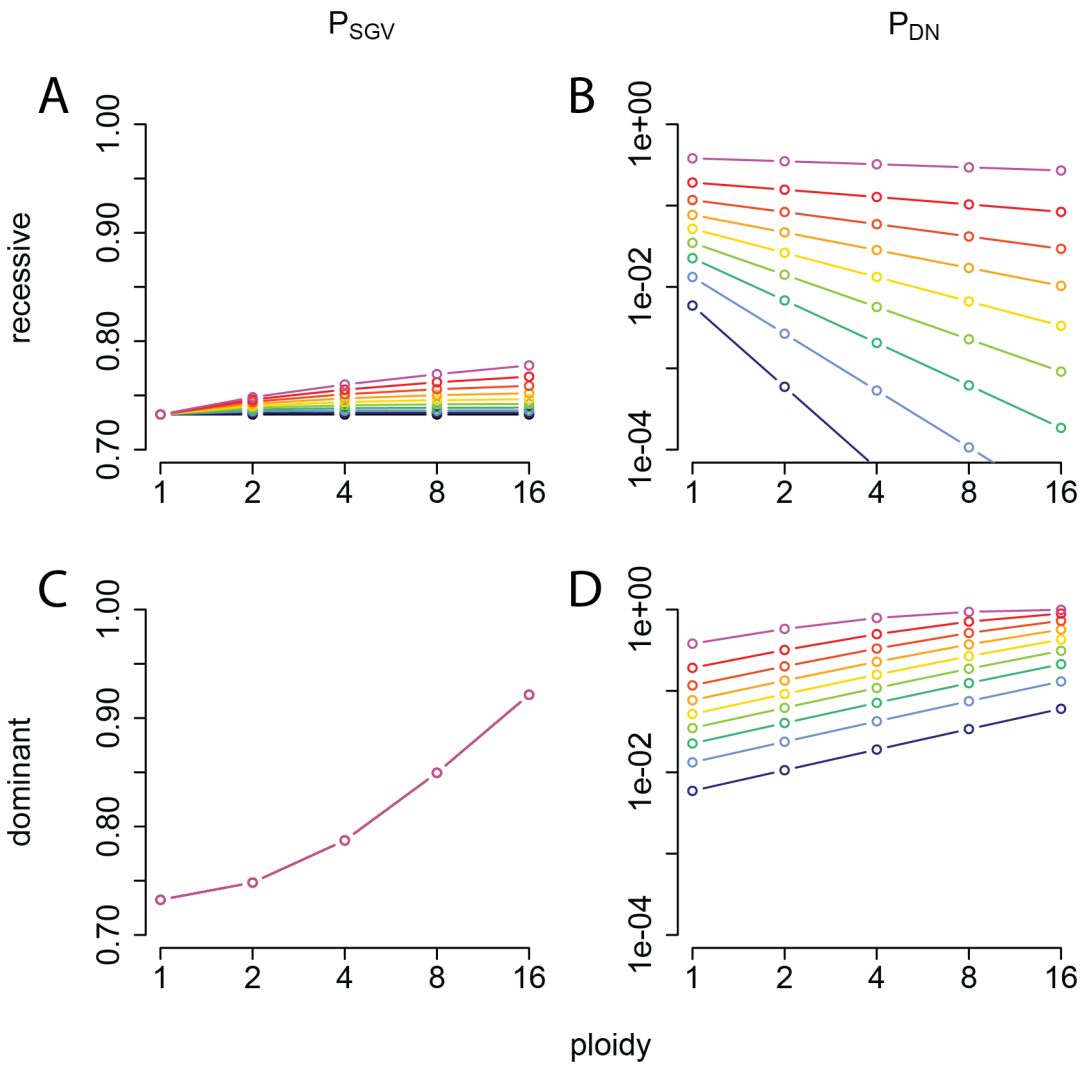

Fig 8. Impact of effective polyploidy on the probability of evolutionary rescue. (A, C) The probability that at least one mutation from the SGV survives in the new environment (P_{SGV}; linear scale) and (B, D) the probability that at least one mutation arises in the new environment and survives (P_{DN}; log scale), plotted as a function of ploidy, for a recessive mutation (A, B) or a dominant mutation (C, D). The different colored curves indicate probability of division before death of phenotypically wild-type (sensitive) cells in the new environment, p_S, varying from 0 (black) to 0.45 (magenta) in increments of 0.05. The remaining parameters are fixed: probability of division before death of phenotypically mutant (resistant) cells, p_R = 0.9; mutational cost in the old environment, s = 0.1; population size at the time the environment changes, $N = 2 \times 10^8$; and per-copy mutation rate, $\tilde{\mu}_c = 3 \times 10^{-10}$. This figure can be reproduced using code deposited on Dryad (http://dx.doi.org/10.5061/dryad.8723t). SGV, standing genetic variation.

https://doi.org/10.1371/journal.pbio.2004644.g008

Polyploidy is often regarded as a transient property limited to fast-growing bacteria, but this view has been challenged in recent years. Though ploidy tends to be higher during exponential growth (up to eight or 16 partial chromosome copies) [9], even during stationary phase, *E. coli* cells contain typically four and up to eight complete chromosome copies [10]. Environmental stresses can also induce multinucleated, polyploid cell filaments [37], in which adaptive mutations must overcome phenotypic delay before allowing population survival in deteriorating environments. A recent study exposing bacteria to low doses of the antibiotic ciprofloxacin showed that resistant bacteria can only emerge from mononucleated offspring

cells that bud off from a long multinucleated cellular filament [37]. This observation can be explained by masking of the mutant phenotype in polyploid, heterozygous cells. Furthermore, obligate polyploid bacterial species ranging from free-living bacteria to clinically relevant pathogens have been discovered across six phyla [22,38,39]. This has, for instance, been recognized as a confounding factor in metagenomic studies of bacterial community structure by marker gene–based analysis [38]. Even within the same bacterial species, ploidy may vary in response to selection, as shown in a previous study that *E. coli* with resistance to camphor vapor also showed increased ploidy [40]. Therefore, we argue that polyploidy is broadly relevant for bacteria and will generally result in phenotypic delay of recessive mutations.

Dominance and polyploidy (whether effective or obligate) together affect the number of mutants observed in fluctuation tests and thus require reinterpretation of mutation rate estimates. Fluctuation tests typically use recessive antibiotic resistance mutations. Encouragingly, we found that the resulting estimates accurately reflect the per–target copy mutation rate, regardless of ploidy. Therefore, studies using fluctuation tests to compare per–target copy mutation rates across different conditions, e.g., [41], remain valid. Similarly, we showed that sequencing-based methods of mutation rate estimation from MA assays reflect per–genome copy rates. Therefore, effective polyploidy does not appear to explain the up to 10-fold difference in mutation rate estimates [31,42] obtained using these two different methods.

Importantly, however, neither method reflects the per-cell mutation rate and thus the total mutational influx in the population, which is proportional to ploidy. Indeed, our models suggest that fluctuation tests with recessive mutations or sequencing-based methods leave no detectable signal of ploidy in the data: that is, a polyploid population is indistinguishable from a monoploid population in these assays, even though their total mutational influx differs by a factor equal to the ploidy. Meanwhile, dominant mutations lead to fundamentally different mutant distributions in the fluctuation test, and neither the per-copy nor the per-cell mutation rate is accurately estimated. In conclusion, mutation rate estimates must be interpreted with caution, regardless of the method used.

The effects of polyploidy on number of mutational targets and phenotypic delay influence the evolutionary potential of populations to escape extinction under sudden environmental change such as antibiotic treatment. In particular, we showed that recessive rescue mutations are increasingly likely to come from the SGV as ploidy increases. This is due to the dual effects of masking the fitness cost of these mutations in the old (antibiotic-free) environment while decreasing the chance that de novo mutations survive in the new (antibiotic) environment until their beneficial phenotype is expressed. Our novel results for rescue are broadly in line with previous theoretical findings on the role of ploidy for adaptation [32] and highlight the point that these considerations are relevant to bacteria as well as eukaryotes.

Our theoretical results rest on several simplifying assumptions. Firstly, we examined only the cases of complete dominance or complete recessivity. More generally, gene dosage effects could result in intermediate dominance; in this case, we expect the effects on mutation rate estimation and rescue probability to be intermediate between the two extremes considered here. Secondly, while we examined rescue via single mutations, if multiple mutations with different dominance were available, populations at different ploidy levels may tend to evolve via different pathways [43]. Furthermore, while we exclusively considered chromosomal mutations, mutations on plasmids, particularly those with high copy number [44], should show similar effects, although segregation patterns and thus time to achieve homozygosity are likely to differ. Finally, models developed thus far have assumed constant ploidy, whereas future modeling efforts could incorporate the dynamically changing and environment-dependent nature of bacterial ploidy.

Given the manifold implications of a multigenerational phenotypic delay, we argue that effective polyploidy and the resulting phenotypic delay are essential factors to consider in future studies of bacterial mutation and adaptation.

Materials and methods

Bacterial strains, antibiotics, and media

All experiments were performed with strains derived from the wild-type *E. coli* MG1655 strain. A complete list of strains can be found in S2 Table. Cells were grown at 30˚C in LB or in M9 media with 0.4% lactose. Antibiotics were purchased from Sigma-Aldrich. To prepare stocks, rifampicin was dissolved in DMSO to 100 mg/ml; nalidixic acid was dissolved in 0.3 M NaOH solution to 30 mg/ml; streptomycin and ampicillin were dissolved in MilliQ water to 100 mg/ml and filter sterilized. Rifampicin, streptomycin, and ampicillin stocks were kept at −20˚C, while nalidixic acid was kept at 4˚C. Ampicillin 100 mg/L was used for maintaining the pSIM6 recombineering plasmid. All antibiotic agar plates were prepared fresh before every experiment.

MIC determination

The MICs of rifampicin, streptomycin, and nalidixic acid were determined by broth dilution method in LB and found to be 12 mg/L, 12 mg/L, and 6 mg/L, respectively.

High-efficiency recombineering

Our recombineering protocol was adapted from previous studies [6,21]. To ensure reproducibility, a detailed step-by-step protocol is provided in S1 Text section 1. In brief, *E. coli* harboring pSIM6 plasmids were grown into early exponential phase before heat activation at 43˚C for 10 minutes to express the recombineering proteins. Activated cells were then repeatedly washed in ice-cold MilliQ water to remove residual salts. Concentrated salt-free cell suspension 50 μl was then mixed with approximately 200 ng of ssDNA before electroporation at 1.8 kV/mm. Immediately after electroporation, cells were resuspended in LB and recovered for 30 min at 30˚C. After this initial recovery, cells were pelleted, then resuspended in fresh LB to continuously grow at 30˚C for subsequent phenotyping.

Quantification of phenotypic delay of resistance mutations

From the resuspended population, approximately 2% of cells were sampled hourly for the first 10 hours and then at 24 hours. A time point at 48 hours was also included to control for factors that potentially prevent phenotypic penetrance from ever reaching 100%, such as low establishment probability of mutant cells. The sampled populations were appropriately diluted for optimal plating onto selective and nonselective plates. Total population size and thus generations elapsed in the sampled cultures was estimated from colony-forming units (CFU) on nonselective plates. To score the frequency of genotypic mutants, we replica-plated all colonies from the nonselective plates to selective plates for each tested time point. The frequency of genotypic mutants, F_g, was determined by the fraction of colonies from nonselective plates that could grow after postponed replica plating onto selective plates. The frequency of phenotypic mutants, F_p, was determined by the ratio of CFU from immediate plating on selective plates versus CFU on nonselective plates. Phenotypic penetrance was defined as $P = F_p \div F_g$. Phenotypic delay was then quantified as the time point at which phenotypic penetrance reaches 50%.

Quantification of homozygosity

To quantify mutant homozygosity, i.e., the fraction of homozygous mutants among all genotypic mutants, we developed a *lacZ*-based visual assay. We constructed bacterial strains with a *lacZ* gene disrupted by a nonsense point mutation (E461X) [8] and inserted the broken *lacZ* within 5 kb of each antibiotic resistance target gene. These strains were subjected to recombineering with an ssDNA carrying the reverse point mutation (X461E) that restored the lac^+ phenotype. The resulting phenotypic mutants were selected on M9-lactose media. Phenotypic mutants become blue on permissive media containing 1 mM IPTG and 40 μg/ml X-gal [5]. Heterozygous mutants with mixed lac^+/lac^- alleles form blue-/white-sectored colonies, whereas homozygous mutants form entirely blue colonies (Fig 2E). Plates with colonies were left at 4˚C for 1 week to allow sufficient development of the blue color but before the blue pigment spreads too far to obscure sectored colonies. Counting sectored (s) and nonsectored (n) blue colonies, we determined mutant homozygosity as $f_{hom} = n/(s+n)$. Comparing f_{hom} to the phenotypic penetrance P thus indicates to what extent phenotypic delay is attributable to effective polyploidy. Colony counting was performed using CellProfiler [45].

Single-cell observations

We constructed a strain with a constitutively expressed *YFP* gene disrupted by 3 consecutive stop codons. Recombineering corrected the stop codons. After electroporation and 30 min recovery at 30˚C, 1 μl of appropriately diluted cell suspension was pipetted onto a small 1.5% UltraPure Low Melting Point agarose pad. After drying the pad for 1 minute, it was deposited upside down in a sealed glass-bottom dish (WillCo Wells, GWST-5040). Time-lapse microscopy was performed with a fully automated Olympus IX81 inverted microscope, with 100X NA1.3 oil objective and Hamamatsu ORCA-flash 4.0 sCMOS camera. For fluorescent imaging, we used a Lumen Dynamics X-Cite120 lamp and Chroma YFP fluorescent filter (NA1028). The sample was maintained at 30˚C by a microscope incubator. Phase-contrast and yellow fluorescence images were captured at 5-minute intervals for 16 hours. The subsequent image analysis was performed with a custom-made MATLAB program (Vanellus, accessible at: http://kiviet.com/research/vanellus.php).

Assessing minimal ploidy

We performed the *lacZ* reporter assay, as described above, for three strains with the *lacZ* gene juxtaposed to each of the antibiotic resistance target genes. After the 30-min recovery following recombineering (before extensive growth), cells were plated directly onto LB agar with IPTG and X-gal. After 24 hours of incubation at 30˚C, entire mutant colonies that contained blue color were picked. We started from colonies closest to the center of each agar plate and expanded outwards to eliminate picking bias. The picked colonies were diluted 10^4- to 10^5-fold in PBS before plating on average about 500 CFUs on fresh LB agar with IPTG and X-gal to infer the fraction of mutant cells in the given colony. This fraction was then used to deduce the minimal ploidy at the time of ssDNA integration based on a previous study [46]: a colony with one-quarter mutant cells, for instance, has minimal ploidy of 2 because it could have resulted from mutagenesis on 1 out of 4 DNA single strands. Actual ploidy may be higher if, for instance, 2 out of 8 single strands mutated in a cell of ploidy 4.

Ploidy and chromosome segregation model

For simplicity, we assumed every cell has the same effective ploidy, i.e., copies of the gene of interest, over the relevant timescale. At each generation, chromosomes must therefore undergo

one round of replication and be evenly divided between the two daughter cells. In *E. coli*, chromosomes appear to progressively separate as they are replicated and detach last at the terminus [9]. We therefore assumed segregation into daughter cells occurs at the most ancestral split in the chromosome genealogy. This assumption is conservative because it implies that mutant chromosomes always remain together, resulting in the fastest possible approach to homozygosity and thus the shortest phenotypic delay. Under this model, ploidy must take the form $c = 2^n$ (for $n = 0, 1, 2, \ldots$), among which the number of mutant copies is $j = 0$ or 2^i ($0 \leq i \leq n$), while the remaining $c–j$ copies are wild-type. Note that other models of segregation are possible, e.g., random segregation in highly polyploid Archaea [28], which would lead to slower approach to homozygosity and corresponding effects on the evolutionary model results.

Simulated fluctuation tests

All simulations and inference were implemented in R. We wrote our own code to account for polyploidy, but in the future, our methods could potentially be integrated into recently published R packages for fluctuation analysis [47,48]. We simulated culture growth in nonselective media with stochastic appearance of spontaneous de novo mutations (for details see S1 Text section 3.1). We assumed a fixed per-copy mutation rate of μ_c per wild-type cell division, such that the per-cell mutation rate is $\mu = c\,\mu_c$ for effective ploidy c. We neglected the chance of more than one copy mutating simultaneously, i.e., mutants always arose with the mutation in a single chromosome copy. Although natural mutations may initially arise in either single- or double-stranded form (for instance, mismatches versus indels following double-strand breaks), to be consistent with the standard model, we assumed mutations arose in double-stranded form (see discussion in S1 Text sections 2.1 and 2.3). The descendants of each de novo mutant were tracked individually, with mutant chromosomes segregating as described above and interdivision times either drawn independently from an exponential distribution or constant. We assumed no fitness differences between wild-type and mutant in nonselective media. In the case of $c = 1$ and exponential interdivision times, our model corresponds to the standard "Lea-Coulson" model [23,30], which is also the basis of the widely used software FALCOR [49].

Each simulated culture was initiated with 1,000 wild-type cells, and after 20 wild-type population doublings, the culture growth phase ended and phenotypic mutants were counted under the assumption of either complete recessivity (requiring all c chromosomes to be mutant) or complete dominance (requiring at least one mutant chromosome). Assuming (as standard) 100% plating efficiency and no growth of phenotypically wild-type cells under selective conditions, the number of colonies formed on selective plates equals the number of phenotypic mutants in the final culture. The mutant colony counts from 50 simulated parallel cultures were then used to obtain a maximum likelihood estimate (MLE) $\hat{\mu}$ and 95% profile likelihood confidence intervals of mutation rate under the standard model, which in particular assumes that a de novo mutant and all its descendants are immediately phenotypically mutant. The best-fitting distribution of mutant counts was calculated from the standard model with mutation rate equal to $\hat{\mu}$. While we implemented these calculations in R (code available on Dryad: http://dx.doi.org/10.5061/dryad.8723t), calculation of the likelihood under this model has been previously described [29,50] and has also been implemented in FALCOR [49].

Mutation–selection balance

We considered a population with effective ploidy c, in which mutations arise (again, in double-stranded form) in a proportion $\tilde{\mu} = c\tilde{\mu}_c$ of offspring in each generation. The definition of mutation rate used in the population genetics literature is subtly different from that used in

fluctuation analysis and thus given different notation here (see S1 Text section 4.1). The mutation has relative fitness cost s in homozygotes, with the cost either completely masked (if recessive) or equal (if dominant) in heterozygotes. We extended deterministic genotype frequency recursions to incorporate chromosome segregation as described above and solved for the equilibrium frequencies of all heterozygous and homozygous mutant types (S1 Text section 4.2).

Evolutionary rescue

We modeled the fate of a population shifted to a harsh new environment, i.e., either extinction or rescue by mutants, stochastically using a multi-type branching process. Unlike in the fluctuation test simulations, where we neglected the chance that wild-type cells produce surviving lineages in the new environment, here we allowed a probability $p_S \leq ½$ that a phenotypically wild-type cell successfully divides before death to produce 2 offspring, while phenotypically mutant cells have corresponding probability $p_R > ½$. Therefore, phenotypically wild-type cells cannot sustain themselves but have a nonzero chance of producing phenotypically mutant descendants either by segregation of mutant alleles in the SGV (modeled by mutation–selection balance as above) or de novo mutations during residual divisions in the new environment. We derived analytical approximations (S1 Text section 4.3) for the probability of rescue from SGV (P_{SGV}) or from de novo mutations (P_{DN}), which are not mutually exclusive.

All data were deposited in the Dryad repository (http://dx.doi.org/10.5061/dryad.8723t) [51].

Supporting information

S1 Text. Supplementary text with detailed recombineering protocol, model descriptions, and mathematical results.
(PDF)

S1 Table. List of mutations used in this study.
(DOCX)

S2 Table. List of bacterial strains used in this study.
(XLSX)

S3 Table. List of oligonucleotides used in this study.
(XLSX)

S1 Data. Numerical values underlying the graphs in Figs 2, 3 and 4 and S10 Fig.
(XLSX)

S1 Fig. Schematic of cell lineage dynamics in a mutant clone. In this illustration, generation times are constant (synchronous division) for simplicity; ploidy $c = 4$ and a mutation arose in one copy. The existence of polyploidy implies that phenotypic mutants initially appear as singletons. For recessive traits, there is a delay of $\log_2 c$ generations after the de novo mutation until a single phenotypic mutant appears, then the number of phenotypic mutants doubles in each subsequent generation. For dominant traits, a single phenotypic mutant appears in the generation that the de novo mutation occurs but remains a singleton for $\log_2 c$ additional generations before the number of phenotypic mutants begins to double. In both cases, in the long term, a fraction $1/c$ of descendants are expected to be homozygous mutants and the rest wild-type.
(TIF)

S2 Fig. Mutation rate estimates from simulated fluctuation tests. For various per-copy mutation rates μ_c (columns), for either constant (top row of each panel) or exponentially distributed (bottom row) interdivision times, and for each ploidy level c, 50 parallel cultures were simulated to make up one experiment. From each simulated culture, phenotypic mutants were counted assuming either (A) a recessive or (B) a dominant trait. This was repeated for two independent experiments (square and triangle symbols) for each parameter set. The MLE of mutation rate and 95% profile likelihood confidence intervals are plotted as a function of ploidy. In each panel, the lower solid black line indicates the actual per-copy mutation rate (μ_c) and the upper black dashes indicate the per-cell mutation rate ($c\mu_c$). The results from the first simulated experiment with $\mu_c = 3 \times 10^{-10}$ and constant interdivision times correspond to the main text Fig 6A and 6B. This figure can be reproduced using code and simulated data deposited on Dryad (http://dx.doi.org/10.5061/dryad.8723t). MLE, maximum likelihood estimate.
(TIF)

S3 Fig. Mutant count distributions from simulated fluctuation tests. At each ploidy level, assuming the trait is either recessive (A) or dominant (B), the observed mutant count across 50 simulated parallel cultures is plotted as a histogram. The simulated data are the same as that used in S2 Fig for the first experiment with per-copy mutation rate $\mu_c = 3 \times 10^{-10}$ and constant interdivision times. The distribution predicted by the standard model, parameterized by the maximum likelihood estimated mutation rate, is also plotted for comparison (connected points). The plots for ploidy $c = 4$ correspond to the main text Fig 6C and 6D. This figure can be reproduced using code and simulated data deposited on Dryad (http://dx.doi.org/10.5061/dryad.8723t).
(TIF)

S4 Fig. Model of a MA experiment. (A) In an MA experiment, a bacterial population evolves for thousands of generations with single-colony bottlenecking every 25 to 30 generations. However, we track only the lineage of direct ancestors leading to the ultimately sampled single cell. (B) In a polyploid cell, acquiring a mutation yields a heterozygous mutant cell. For this mutation to fix in the sampled lineage and be detected by WGS, the daughter cell inheriting the mutant copies must be chosen at each cell division for further propagation in the sampled lineage. (C) Asymmetric inheritance caused by polyploidy reduces the fixation probability of mutations because the daughter cell inheriting the mutation may not be sampled. MA, mutation accumulation; WGS, whole-genome sequencing.
(TIF)

S5 Fig. Mutant allele frequency at mutation–selection balance. The frequency of the mutant allele is plotted as a function of its cost s, in the case of a completely recessive (A) or completely dominant (B) allele. In this example, ploidy $c = 2^n = 8$ and per-copy mutation rate $\tilde{\mu}_c = 3 \times 10^{-10}$. The contribution to this frequency made by each cell type (given by $(2^i/2^n)x^*_{2^i}$ in cells containing 2^i mutant chromosomes) is represented by the shaded area between two curves, working up from the bottom through heterozygotes ($0 \leq i \leq n$-1) and then homozygotes ($i = n$). This figure can be reproduced using code deposited on Dryad (http://dx.doi.org/10.5061/dryad.8723t).
(TIF)

S6 Fig. Probability of rescue with a recessive mutation as a function of probabilities of cell division before death. From left to right: probability of rescue from SGV, P_{SGV}; from de novo mutations, P_{DN}; from either or both, P_{tot}; and the ratio of probabilities, P_{SGV}/P_{DN} (on log

scale). The missing values (white) occur where $P_{DN} = 0$ and the ratio is undefined. All quantities are plotted as functions of the probabilities of division before death of sensitive cells (p_S; horizontal axis) and resistant cells (p_R; vertical axis). Ploidy (c) varies by row as indicated. Additional model parameters $s = 0.1$ and $m = 0.06$ are fixed. This figure can be reproduced using code deposited on Dryad (http://dx.doi.org/10.5061/dryad.8723t). SGV, standing genetic variation.
(TIF)

S7 Fig. Probability of rescue with a dominant mutation as a function of probabilities of cell division before death. All plotting parameters are identical to S6 Fig. This figure can be reproduced using code deposited on Dryad (http://dx.doi.org/10.5061/dryad.8723t).
(TIF)

S8 Fig. Probability of rescue with a recessive mutation as a function of mutational influx and cost. From left to right: probability of rescue from SGV, P_{SGV}; from de novo mutations, P_{DN}; from either or both, P_{tot}; and the ratio of probabilities, P_{SGV}/P_{DN} (on log scale). All quantities are plotted as functions of the base-10 log of mutational influx ($\log_{10}(m) = \log_{10}(N\tilde{\mu}_c)$; horizontal axis in each plot) and the cost of the mutation in the old environment (s; vertical axis in each plot). Ploidy (c) varies by row as indicated. Additional model parameters $p_S = 0.2$ and $p_R = 0.9$ are fixed. This figure can be reproduced using code deposited on Dryad (http://dx.doi.org/10.5061/dryad.8723t). SGV, standing genetic variation.
(TIF)

S9 Fig. Probability of rescue with a dominant mutation as a function of mutational influx and cost. All plotting parameters are identical to S8 Fig. This figure can be reproduced using code deposited on Dryad (http://dx.doi.org/10.5061/dryad.8723t).
(TIF)

S10 Fig. An example of a growth curve from the phenotypic delay experiments. The illustrated growth curve is from the Rif^R recombineering experiment. Sampling occurred during the first 10 hours after recombineering, with the first sample taken at 0.5 h immediately after recovery from electroporation. Population doublings, expressed in number of generations after the first sampling time point, is calculated based on CFU counts at each sampling time. Red dots indicate individual data points from each of six replicates sampled at each time. The black line shows a linear regression of how generation time depends on real time expressed in hours, fitted through the mean of the replicates at each time point. The numerical values can be found in S1 Data. CFU, colony-forming unit.
(TIF)

S1 Movie. Time-lapse film of the bacterial microcolony shown in Fig 3A.
(MP4)

Acknowledgments

We thank Erik Wistrand-Yuen, Erik Lundin, and Gerrit Brandis from the groups of Dan I. Andersson and Diarmaid Hughes at Uppsala University for kindly gifting us some bacterial strains and plasmids. We also thank Sébastien Wielgoss, Gabriel Leventhal, Andrew Read, and Min Wu for helpful discussions.

Author Contributions

Conceptualization: Lei Sun, Helen K. Alexander, Martin Ackermann, Sebastian Bonhoeffer.

Formal analysis: Lei Sun, Helen K. Alexander, Balazs Bogos, Daniel J. Kiviet.

Funding acquisition: Martin Ackermann, Sebastian Bonhoeffer.

Investigation: Lei Sun, Helen K. Alexander, Balazs Bogos, Daniel J. Kiviet.

Methodology: Lei Sun, Helen K. Alexander, Balazs Bogos, Daniel J. Kiviet.

Project administration: Sebastian Bonhoeffer.

Software: Helen K. Alexander, Balazs Bogos, Daniel J. Kiviet.

Supervision: Martin Ackermann, Sebastian Bonhoeffer.

Writing – original draft: Lei Sun, Helen K. Alexander, Sebastian Bonhoeffer.

Writing – review & editing: Lei Sun, Helen K. Alexander, Balazs Bogos, Daniel J. Kiviet, Martin Ackermann, Sebastian Bonhoeffer.

References

1. Luria SE, Delbrück M. Mutations of bacteria from virus sensitivity to virus resistance. Genetics. 1943; 28: 491–511. PMID: 17247100
2. Ryan FJ. Phenotypic (phenomic) lag in bacteria. Am Nat. 1955; 89: 159–162.
3. Newcombe HB. Delayed phenotypic expression of spontaneous mutations in Escherichia coli. Genetics. 1948; 33.
4. Kendal WS, Frost P. Pitfalls and Practice of Luria-Delbruck Fluctuation Analysis: A Review. Cancer Res. 1988; 48: 1060–1065. PMID: 3277705
5. Sambrook J, Green MR. Molecular Cloning—A Laboratory Manual 4th Edition. Cold Spring Harbor Laboratory Press; 2012.
6. Sharan SK, Thomason LC, Kuznetsov SG, Court DL. Recombineering: a homologous recombination-based method of genetic engineering. Nat Protoc. 2009; 4: 206–23. https://doi.org/10.1038/nprot.2008.227 PMID: 19180090
7. Trindade S, Sousa A, Xavier KB, Dionisio F, Ferreira MG, Gordo I. Positive epistasis drives the acquisition of multidrug resistance. PLoS Genet. 2009; 5: e1000578. https://doi.org/10.1371/journal.pgen.1000578 PMID: 19629166
8. Cupples CG, Miller JH. A set of lacZ mutations in Escherichia coli that allow rapid detection of each of the six base substitutions. Proc Natl Acad Sci. 1989; 86: 5345–5349. PMID: 2501784
9. Nielsen HJ, Youngren B, Hansen FG, Austin S. Dynamics of Escherichia coli chromosome segregation during multifork replication. J Bacteriol. 2007; 189: 8660–8666. https://doi.org/10.1128/JB.01212-07 PMID: 17905986
10. Akerlund T, Nordström K, Bernander R. Analysis of cell size and DNA content in exponentially growing and stationary-phase batch cultures of Escherichia coli. J Bacteriol. 1995; 177: 6791–6797. PMID: 7592469
11. Edgar R, Friedman N, Molshanski-Mor S, Qimron U. Reversing bacterial resistance to antibiotics by phage-mediated delivery of dominant sensitive genes. Appl Environ Microbiol. 2012; 78: 744–51. https://doi.org/10.1128/AEM.05741-11 PMID: 22113912
12. Hayward RS. DNA Blockade by Rifampicin-Inactivated Escherichia coli RNA Polymerase, and Its Amelioration by a Specific Mutation. Eur J Biochem. 1976; 71: 19–24. PMID: 795662
13. Cirz RT, Chin JK, Andes DR, de Crécy-Lagard V, Craig W a, Romesberg FE. Inhibition of mutation and combating the evolution of antibiotic resistance. PLoS Biol. 2005; 3: e176. https://doi.org/10.1371/journal.pbio.0030176 PMID: 15869329
14. Palmer AC, Kishony R. Opposing effects of target overexpression reveal drug mechanisms. Nat Commun. 2014; 5: 4296.
15. Nagel R, Chan A. Mistranslation and genetic variability. The effect of streptomycin. Mutat Res—Fundam Mol Mech Mutagen. 2006; 601: 162–170.
16. Ovchinnikov YA, Monastyrskaya GS, Guriev SO, Kalinina NF, Sverdlov ED, Gragerov AI, et al. RNA polymerase rifampicin resistance mutations in Escherichia coli: Sequence changes and dominance. Mol Gen Genet. 1983; 190: 344–348. PMID: 6348476

17. Kremers G-J, Goedhart J, van Munster EB, Gadella TWJ. Cyan and yellow super fluorescent proteins with improved brightness, protein folding, and FRET Förster radius. Biochemistry. 2006; 45: 6570–80. https://doi.org/10.1021/bi0516273 PMID: 16716067

18. Boyle NR, Reynolds TS, Evans R, Lynch M, Gill RT. Recombineering to homogeneity: Extension of multiplex recombineering to large-scale genome editing. Biotechnol J. 2013; 8: 515–522. https://doi.org/10.1002/biot.201200237 PMID: 23436787

19. Adiciptaningrum AM, Blomfield IC, Tans SJ. Direct observation of type 1 fimbrial switching. EMBO Rep. 2009; 10: 527–532. https://doi.org/10.1038/embor.2009.25 PMID: 19325559

20. Calvin NM, Hanawalt PC. High-Efficiency Transformation of Bacterial cells by Electroporation. J Bacteriol. 1988; 170: 2796–2801. PMID: 3286620

21. Sawitzke JA, Thomason LC, Costantino N, Bubunenko M, Datta S, Court DL. Recombineering: In Vivo Genetic Engineering in E. coli, S. enterica, and Beyond. Methods Enzymol. 2007; 421: 171–199. https://doi.org/10.1016/S0076-6879(06)21015-2 PMID: 17352923

22. Tobiason DM, Seifert HS. The Obligate Human Pathogen, Neisseria gonorrhoeae, Is Polyploid. PLoS Biol. 2006; 4: e185. https://doi.org/10.1371/journal.pbio.0040185 PMID: 16719561

23. Foster PL. Methods for determining spontaneous mutation rates. Methods Enzymol. 2006; 409: 195–213. https://doi.org/10.1016/S0076-6879(05)09012-9 PMID: 16793403

24. Kondo S. A theoretical study on spontaneous mutation rate. Mutat Res. 1972; 240: 365–374.

25. Ryan FJ, Wainwright LK. Nuclear segregation and the growth of clones of spontaneous mutants of bacteria. J Gen Microbiol. 1954; 11: 364–379. https://doi.org/10.1099/00221287-11-3-364 PMID: 13221757

26. Lederberg J. Aberrant heterozygotes in Escherchia coli. Proc Natl Acad Sci. 1949; 35: 178–184. PMID: 16588878

27. Kissling GE, Grogan DW, Drake JW. Confounders of mutation-rate estimators: Selection and phenotypic lag in Thermus thermophilus. Mutat Res—Fundam Mol Mech Mutagen. 2013; 749: 16–20.

28. Markov AV, Kaznacheev IS. Evolutionary consequences of polyploidy in prokaryotes and the origin of mitosis and meiosis. Biol Direct. 2016; 11: 1–22.

29. Zheng Q. Statistical and algorithmic methods for fluctuation analysis with SALVADOR as an implementation. Math Biosci. 2002; 176: 237–252. PMID: 11916511

30. Zheng Q. Progress of a half century in the study of the Luria-Delbrück distribution. Math Biosci. 1999; 162: 1–32. PMID: 10616278

31. Lee H, Popodi E, Tang H, Foster PL. Rate and molecular spectrum of spontaneous mutations in the bacterium Escherichia coli as determined by whole-genome sequencing. Proc Natl Acad Sci. 2012; 109: E2774–E2783. https://doi.org/10.1073/pnas.1210309109 PMID: 22991466

32. Otto SP, Whitton J. Polyploid incidence and evolution. Annu Rev Genet. 2000; 34: 401–437. https://doi.org/10.1146/annurev.genet.34.1.401 PMID: 11092833

33. Orr HA, Otto SP. Does diploidy increase the rate of adaptation? Genetics. 1994; 136: 1475–1480. PMID: 8013920

34. Ribeiro RM, Bonhoeffer S. Production of resistant HIV mutants during antiretroviral therapy. Proc Natl Acad Sci. 2000; 97: 7681–7686. PMID: 10884399

35. Barrett RDH, Schluter D. Adaptation from standing genetic variation. Trends Ecol Evol. 2008; 23: 38–44. https://doi.org/10.1016/j.tree.2007.09.008 PMID: 18006185

36. Alexander HK, Martin G, Martin OY, Bonhoeffer S. Evolutionary rescue: Linking theory for conservation and medicine. Evol Appl. 2014; 7: 1161–1179. https://doi.org/10.1111/eva.12221 PMID: 25558278

37. Bos J, Zhang Q, Vyawahare S, Rogers E, Rosenberg SM, Austin RH. Emergence of antibiotic resistance from multinucleated bacterial filaments. Proc Natl Acad Sci. 2015; 112: 178–83. https://doi.org/10.1073/pnas.1420702111 PMID: 25492931

38. Soppa J. Polyploidy and community structure. Nat Microbiol. 2017; 2: 16261. https://doi.org/10.1038/nmicrobiol.2016.261 PMID: 28120929

39. Angert ER. DNA Replication and Genomic Architecture of Very Large Bacteria. Annu Rev Microbiol. 2012; 66: 197–212. https://doi.org/10.1146/annurev-micro-090110-102827 PMID: 22994492

40. Trun NJ, Gottesman S. On the bacterial cell cycle: Escherichia coli mutants with altered ploidy. Genes Dev. 1990; 4: 2036–2047. PMID: 2176633

41. Krašovec R, Richards H, Gifford DR, Hatcher C, Faulkner KJ, Belavkin RV, et al. Spontaneous mutation rate is a plastic trait associated with population density across domains of life. PLoS Biol. 2017; 15: e2002731. https://doi.org/10.1371/journal.pbio.2002731 PMID: 28837573

42. Wielgoss S, Barrick JE, Tenaillon O, Cruveiller S, Chane-Woon-Ming B, Médigue C, et al. Mutation Rate Inferred From Synonymous Substitutions in a Long-Term Evolution Experiment With Escherichia coli. G3. 2011; 1: 183–186. https://doi.org/10.1534/g3.111.000406 PMID: 22207905

43. Anderson JB, Sirjusingh C, Ricker N. Haploidy, diploidy and evolution of antifungal drug resistance in Saccharomyces cerevisiae. Genetics. 2004; 168: 1915–1923. https://doi.org/10.1534/genetics.104.033266 PMID: 15371350

44. Santos-Lopez A, Bernabe-Balas C, Ares-Arroyo M, Ortega-Huedo R, Hoefer A, Millan AS, et al. A Naturally Occurring Single Nucleotide Polymorphism in a Multicopy Plasmid Produces a Reversible Increase in Antibiotic Resistance. Antimicrob Agents Chemother. 2017; 61: e01735–16.

45. Jones TR, Kang IH, Wheeler DB, Lindquist RA, Papallo A, Sabatini DM, et al. CellProfiler Analyst: data exploration and analysis software for complex image-based screens. BMC Bioinformatics. 2008; 9: 482. https://doi.org/10.1186/1471-2105-9-482 PMID: 19014601

46. Sawitzke JA, Costantino N, Li X-T, Thomason LC, Bubunenko M, Court C, et al. Probing cellular processes with oligo-mediated recombination and using the knowledge gained to optimize recombineering. J Mol Biol. Elsevier B.V.; 2011; 407: 45–59.

47. Mazoyer A, Drouilhet R, Despréaux S, Ycart B. flan: An R Package for Inference on Mutation Models. R J. 2017; 9: 334–351.

48. Zheng Q. rSalvador: An R Package for the Fluctuation Experiment. G3. 2017; 7: 3849–3856. https://doi.org/10.1534/g3.117.300120 PMID: 29084818

49. Hall BM, Ma C-X, Liang P, Singh KK. Fluctuation analysis CalculatOR: a web tool for the determination of mutation rate using Luria-Delbrück fluctuation analysis. Bioinformatics. 2009; 25: 1564–5. https://doi.org/10.1093/bioinformatics/btp253 PMID: 19369502

50. Sarkar S, Ma WT, Sandri GH. On fluctuation analysis: a new, simple and efficient method for computing the expected number of mutants. Genetica. 1992; 85: 173–179. PMID: 1624139

51. Sun L, Alexander HK, Bogos B, Kiviet DJ, Ackermann M, Bonhoeffer S. Data from: Effective polyploidy causes phenotypic delay and influences bacterial evolvability. In: Dryad Digital Repository [Internet]. 2018. [Cited on 15 February 2018]. http://dx.doi.org/10.5061/dryad.8723t.